Supporting Information

Sustainable plasma-catalytic bubbles for hydrogen peroxide synthesis

Renwu Zhou,[a#*] Tianqi Zhang,[a#] Rusen Zhou,[a,b*] Sen Wang,[c] Danhua Mei,[c] Anne Mai-Prochnow,[a] Janith Weerasinghe,[b] Zhi Fang,[c] Kostya (Ken) Ostrikov,[b] and Patrick J Cullen[a]

[a] Australia. School of Chemical and Biomolecular Engineering, The University of Sydney, NSW 2006, Australia

[b] School of Chemistry and Physics, Center for Materials Science, Queensland University of Technology, Brisbane, QLD 4000, Australia

[c] College of Electrical Engineering and Control Science, Nanjing Tech University, Nanjing 210009, China

[#] Renwu Zhou and Tianqi Zhang contributed equally to this work.

*Corresponding author: renwu.zhou@sydney.edu.au and zhourusen2008@gmail.com

Table S1. Observed OES data of the argon emission spectral lines. Transition, initial energy levels (E_i) and final energy levels (E_f) taken from Ref [S1].

Wavelength (nm)	Transition	Relative intensity (a.u)		E_i (eV)	E_f (eV)
		Glow	Spark		
696	$2p_2 \rightarrow 1s_5$	10272	21766	13.33	11.55
707	$2p_3 \rightarrow 1s_5$	1253	7310	13.30	11.55
715	$2p_5 \rightarrow 1s_5$	293	882	13.28	11.55
727	$2p_2 \rightarrow 1s_4$	2213	4510	13.33	11.62
738	$2p_3 \rightarrow 1s_4$	2126	12921	13.30	11.62
750	$2p_1 \rightarrow 1s_2$	3598	13356	13.48	11.83
751	$2p_5 \rightarrow 1s_4$	2732	12397	13.27	11.62
763	$2p_6 \rightarrow 1s_5$	21579	32181	13.17	11.55
772	$2p_2 \rightarrow 1s_3$	12848	31266	13.15	11.55
795	$2p_4 \rightarrow 1s_3$	3368	15110	13.28	11.72
801	$2p_6 \rightarrow 1s_4$	2761	14587	13.09	11.55
810	$2p_7 \rightarrow 1s_4$	9053	32879	13.15	11.62
811	$2p_9 \rightarrow 1s_5$	3194	22376	13.08	11.55
826	$2p_2 \rightarrow 1s_2$	5777	14892	13.33	11.83
841	$2p_3 \rightarrow 1s_2$	4211	14413	13.30	11.83
842	$2p_8 \rightarrow 1s_4$	1772	21505	13.09	11.62
852	$2p_4 \rightarrow 1s_2$	935	5872	13.28	11.83
866	$2p_2 \rightarrow 1s_5$	207	1405	13.33	11.55

Table S2. Chemical reactions involved in our argon plasma bubble system mainly referred to or partly adapted from Refs.

	Reaction	Reaction rate coefficient	Reference
Gas-phase reaction			
1	$Ar + e^- \rightarrow Ar + e^-$	$2.336 \times 10^{-14} \times T_e^{1.609} \times \exp(0.0618(\ln T_e)^2 - 0.1171(\ln T_e)^3)$	S2
2	$Ar + e^- \rightarrow Ar^* + e^-$	$5 \times 10^{-15} \exp(-12.64/T_e)$	S2
3	$Ar + e^- \rightarrow Ar^+ + 2e^-$	$2.3 \times 10^{-14} T_e^{0.59} \exp(-17.44/T_e)$	S2
4	$Ar^* + e^- \rightarrow Ar^+ + 2e^-$	$6.8 \times 10^{-15} T_e^{0.67} \exp(-4.2/T_e)$	S2
5	$Ar^* + Ar^* \rightarrow Ar^+ + Ar + e^-$	6.4×10^{-16}	S2
6	$Ar^* + e^- \rightarrow Ar + e^-$	$0.5 \times 10^{-15} \exp(-1.09/T_e)$	S2
7	$Ar^* + Ar \rightarrow Ar + Ar$	7.39×10^{-21}	S2
8	$H_2O + e^- \rightarrow H_2O + e^-$	6.0×10^{-13}	S2
9	$H_2O + e^- \rightarrow H_2O^+ + 2e^-$	$9.028 \times 10^{-17} T_e^{2.329} \exp(-11.27/T_e)$	S2
10	$H_2O + e^- \rightarrow \cdot OH + \cdot H + e^-$	$5.526 \times 10^{-14} T_e^{-0.343} \exp(-14.06/T_e)$	S2
11	$H_2O + e^- \rightarrow \cdot OH + H^-$	$2.53 \times 10^{-15} T_e^{-1.199} \exp(-6.12/T_e)$	S2
12	$Ar^* + H_2O \rightarrow Ar + \cdot OH + \cdot H$	4.5×10^{-10}	S2
13	$\cdot OH + \cdot OH \rightarrow H_2O_2$	1.78×10^{-11}	S3
14	$\cdot OH + HO_2 \rightarrow H_2O + O_2$	$4.38 \times 10^{-17} \exp(110.9/T_g)$	S3
15	$\cdot OH + H_2O_2 \rightarrow H_2O + \cdot HO_2$	$4.53 \times 10^{-18} \exp(-288.9/T_g)$	S3
Liquid-phase reaction		Reaction constant ($M^{-1}\ s^{-1}$)	
16	$e_{gas} + H_2O \rightarrow e_{aq} + H_2O$	2×10^9	S3
17	$\cdot OH_g + H_2O \rightarrow \cdot OH_{aq} + H_2O$	3×10^6	S3
18	$\cdot OH_{aq} + \cdot OH_{aq} \rightarrow H_2O_{2aq}$	5×10^9	S4
19	$e_{aq} + H_2O^+ \rightarrow \cdot H + \cdot OH$	6×10^{11}	S3
20	$e_{aq} + H_2O \rightarrow \cdot H + OH^-$	1.9×10^1	S3
21	$e_{aq} + e_{aq} + 2H_2O \rightarrow H_2 + 2OH^-$	$1.0 \times 10^8\ M^{-3}s^{-1}$	S3
22	$\cdot OH_{aq} + \cdot HO_2 \rightarrow H_2O + O_2$	7×10^9	S4
23	$\cdot OH_{aq} + H_2O_2 \rightarrow \cdot HO_2 + H_2O$	2.7×10^7	S4
24	$\cdot OH_{aq} + \cdot H \rightarrow H_2O$	7×10^9	S4
25	$\cdot HO_2 + \cdot HO_2 \rightarrow H_2O_2 + O_2$	8.6×10^5	S4
27	$\cdot HO_2 + H_2O_2 \rightarrow \cdot OH + O_2 + H_2O$	0.5	S4
28	$H_2O_2 \leftrightarrow HO_2^- + H^+$	N/A	
Photo reactions		Reaction constant (cm^2)	
29	$h\nu + H_2O \rightarrow H_3O^+ + e_{aq}$	1×10^{-20}	S3
30	$h\nu + H_2O \rightarrow \cdot H + \cdot OH$	1×10^{-20}	S3

Table S3. Electrical parameters of plasma reactors (c).

Reactors	Voltage amplitude (kV)	Current amplitude (A)	Power (W)
SRGD	6.34	0.25	18.00
SRSD	6.25	0.26	18.11
SRGSD	6.10	0.33	18.25
DRGSD	5.19	0.38	18.25

Table S4. Comparison of catalysts employed in plasma-catalysis system for H_2O_2 production.

Techniques	Operating Conditions	H_2O_2 production rate (mg h^{-1})	Energy Efficiency (g kWh^{-1})	Ref.
Pulsed discharge + TiO_2 nanotubes	Applied voltage: 20 kV; Repetition rate: 100 Hz; Ambient air	1.6	1.1	[S1]
Dielectric barrier discharge + persulfate	Applied voltage: 17 kV; Discharge power: 3.3 (Air plasma) and 5.8 W (Ar plasma);	0.4 (Air plasma) 2.3 (Ar plasma)	0.12 (Air plasma); 0.39 (Ar plasma)	[S2]
Dielectric barrier discharge + Bi_2WO_6-γMoS_2	Applied voltage: 9 kV; Ambient air	2.6	--	[S3]
Gas surface discharge plasma + persulfate	Applied voltage: 7 kV; Repetition rate: 6 kHz ; Air flow rate: 1.0 L/min	27.0	--	[S4]
Pulsed discharge + Graphene-TiO_2 nanocomposite	Applied voltage: 18 kV; Repetition rate: 50 Hz ; Air flow rate: 4 L/min	5.9	0.65	[S5]
Pulsed discharge + TiO_2/WO_3 nanocomposite	Applied voltage: 18 kV; Repetition rate: 50 Hz ; Air flow rate: 4 L/min	5.6	0.62	[S6]
Underwater plasma bubbles + 2D-TiO_2/g-C_3N_4	Discharge power: 18 W; Ar flow rate: 1 L/min	76.5 (DRGSD) 164.6 (DRGSD+2D-TiO_2/g-C_3N_4)	4.2 (DRGSD) 9.0 (DRGSD+2D-TiO_2/g-C_3N_4)	This work

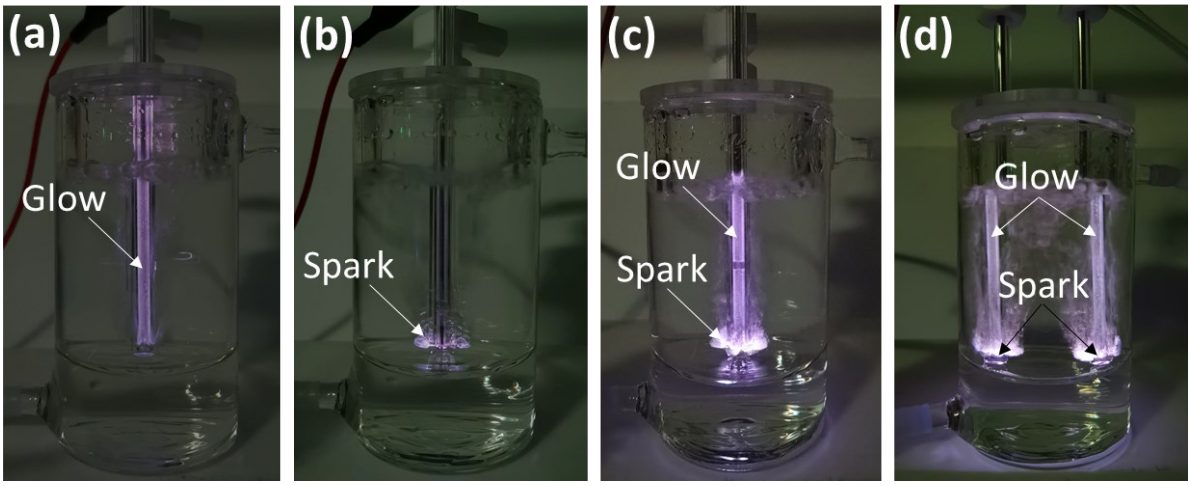

Fig. S1 Photographs of plasma bubble column reactors design configurations: (a) single reactor glow discharge (SRGD); (b) single reactor spark discharge (SRSD); (c) single reactor glow and spark discharge (SRGSD); (d) double reactor glow and spark discharge (DRGSD).

To achieve the SRGD, the high voltage electrode was sheathed with the sealed quartz tubes. The latter incorporated an unsealed quartz tubes to induce a spark extending longitudinally towards the bubbles. Meanwhile, combinative discharge schemes were achieved in the SRGSD reactor with a bare electrode. In the configuration involving the single reactor, the circuit was completed by connecting the negative tungsten rod immerged in water, while for the double reactors, the second reactor was connected to the negative terminal.

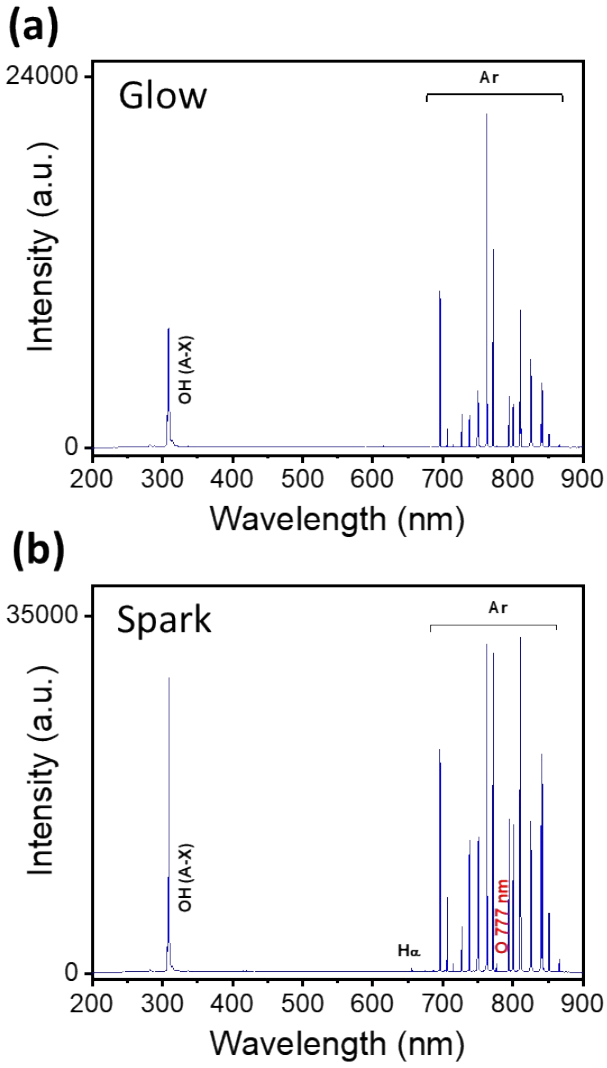

Fig. S2 Optical Emission Spectra (OES) measurements representing (a) the glow discharge and (b) spark discharge.

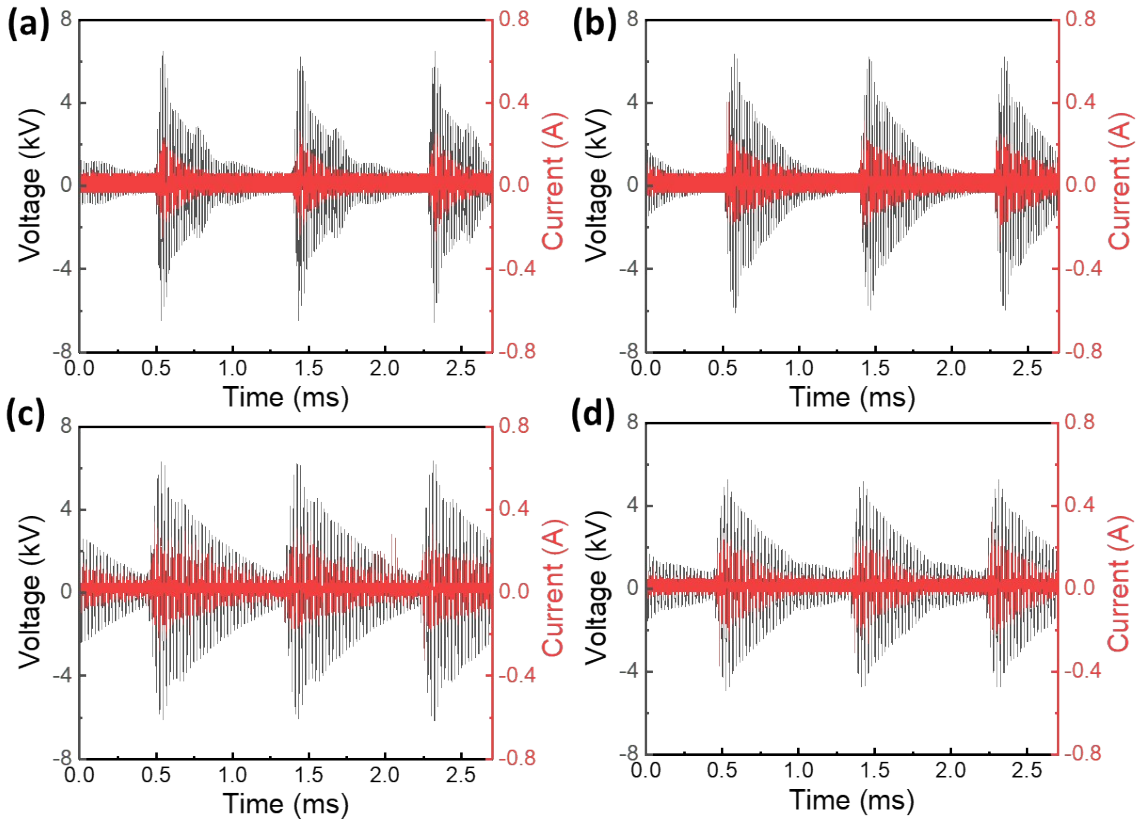

Fig. S3 Electrical diagnostic data for (a) single reactor glow discharge (SRGD); (b) single reactor spark discharge (SRSD); (c) single reactor glow and spark discharge (SRGSD); (d) double reactor glow and spark discharge (DRGSD).

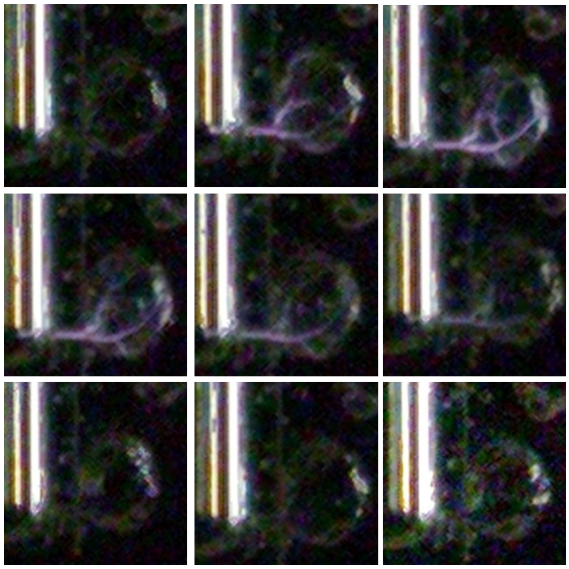

Fig. S4 Dynamic process of plasma discharge propagation in bubbles over one cycle.

To further understand the transformation of the electrical power, the behaviors of the bubbles were recorded by an ultra-speed camera (Nova S16, with the frame rate set at 66 K fps) in a free run mode. As shown in Fig. S4, the discharge was initially initiated at the electrode-side of the bubble where the electric field enhancement is prevalent, and subsequently, the streamer propagated along the surface of the bubbles. The streamer channel expanded to a maximum size before beginning to shrink. Finally, fine bubbles formed, delivering the species into the aqueous solution.

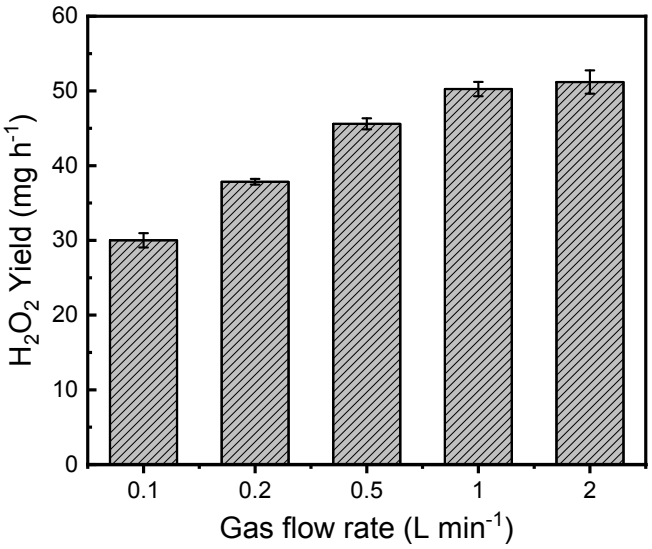

Fig. S5 The effect of gas flow rate on H_2O_2 production using SRGSD (8 holes, 18 W and dry feeding gas).

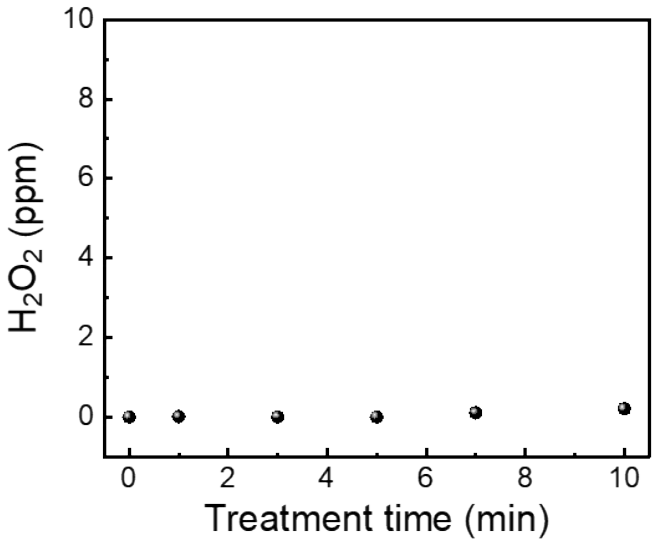

Fig. S6 Concentration of H_2O_{2aq} produced by the plasma-induced photolysis of water as a function of the treatment time. In order to only treat the solutions with plasma-produced UV irradiation, other plasma species are excluded by using a plasma column without any microholes.

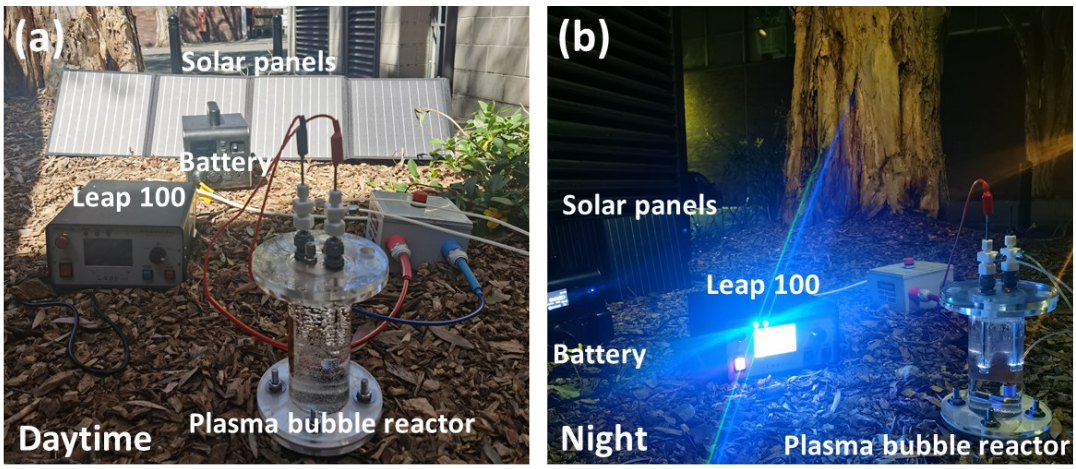

Fig. S7 Photos of solar-powered plasma bubble reactor system taken at daytime and night.

Reference

[S1] A. Kramida, Y. Ralchenko and J. Reader, NIST Atomic Spectra Database (ver. 5.2). (National Institute of Standards and Technology, Gaithersburg, MD, 2015). (Available at: http://physics.nist.gov/asd, date last accessed April 28, 2015).

[S2] D. Liu, B. Sun, F. Iza, D. Xu, X. Wang, M. Rong, M. Kong, *Plasma Sources Science and Technology*, 2017, **26**, 045009.

[S3] W. Tian, M. J. Kushner, *Journal of Physics D: Applied Physics*, 2014, **47**, 165201.W.

[S4] Z. C. Liu, D. X. Liu, C. Chen, D. Li, A. J. Yang, M. Z. Rong, H. L. Chen, M. G. Kong, *Journal of Physics D: Applied Physics*, 2015, **48**, 495201.

[S5] Y. Zhang, Q. Xin, Y. Cong, Q. Wang and B. Jiang, *Chemical Engineering Journal*, 2013, **215**, 261-268.

[S6] K. Shang, X. Wang, J. Li, H. Wang, N. Lu, N. Jiang and Y. Wu, *Chemical Engineering Journal*, 2017, **311**, 378-384.

[S7] K. Zheng, Y. Sun, S. Gong, G. Jiang, X. Zheng and Z. Yu, *Chemosphere*, 2019, **222**, 872-883.

[S8] S. Tang, D. Yuan, Y. Rao, N. Li, J. Qi, T. Cheng, Z. Sun, J. Gu and H. Huang, *Chemical Engineering Journal*, 2018, **337**, 446-454.

[S9] H. Guo, N. Jiang, H. Wang, K. Shang, N. Lu, J. Li and Y. Wu, *Applied Catalysis B: Environmental*, 2019, **248**, 552-566.

[S10] H. Guo, N. Jiang, H. Wang, N. Lu, K. Shang, J. Li and Y. Wu, *Journal of hazardous materials*, 2019, **371**, 666-676.